Automating Multi-Throw Multilateral Surgical Suturing with a Mechanical Needle Guide and Sequential Convex Optimization

Siddarth Sen*[1], Animesh Garg*[2], David V. Gealy[3], Stephen McKinley[3], Yiming Jen[1], Ken Goldberg[2]

Abstract— For supervised automation of multi-throw suturing in Robot-Assisted Minimally Invasive Surgery, we present a novel mechanical needle guide and a framework for optimizing needle size, trajectory, and control parameters using sequential convex programming. The Suture Needle Angular Positioner (SNAP) results in a 3x error reduction in the needle pose estimate in comparison with the standard actuator. We evaluate the algorithm and SNAP on a da Vinci Research Kit using tissue phantoms and compare completion time with that of humans from the JIGSAWS dataset [5]. Initial results suggest that the dVRK can perform suturing at 30% of human speed while completing 86% suture throws attempted. Videos and data are available at: **berkeleyautomation.github.io/amts**

I. Introduction

Robotic Surgical Assistants (RSA), such as Intuitive Surgical's da Vinci System have facilitated over $570,000$ procedures worldwide in 2014 [7]. RSAs are currently controlled by surgeons using pure tele-operation. Automation of surgical sub-tasks such as suturing has the potential to reduce surgeon tedium and fatigue, operating time, and enable supervised tele-surgery.

The Fundamental Skills of Robotic Surgery (FSRS) defines a representative set of procedures for surgical training and evaluation [35]. FSRS includes Multi-Throw Suturing (MTS) where each MTS throw includes five steps as illustrated in Figure 1. A curved needle with suture thread is repeatedly pushed through a pair of tissue boundaries with one actuator, then pulled through with a second actuator until the thread is taut, then is transferred back to the first actuator to begin the next throw / suture [1, 6]. In Robot-Assisted Minimally Invasive Surgery (RMIS), MTS is a tedious subtask and it can be difficult for the surgeon to maintain proper needle pose during insertion and transfer as haptic feedback is not available.

In this paper, we present initial results toward automating MTS with new hardware and a novel optimization algorithm. Our approach includes (1) a mechanical device, the Suture Needle Angular Positioner (SNAP), designed to align and hold the needle in a known orientation, (2) computer vision software to track needle pose, and (3) a sequential convex optimization formulation of needle motion planning. Initial results suggest that SNAP can reduce error in needle orientation by $3\times$ and that the combined system can successfully
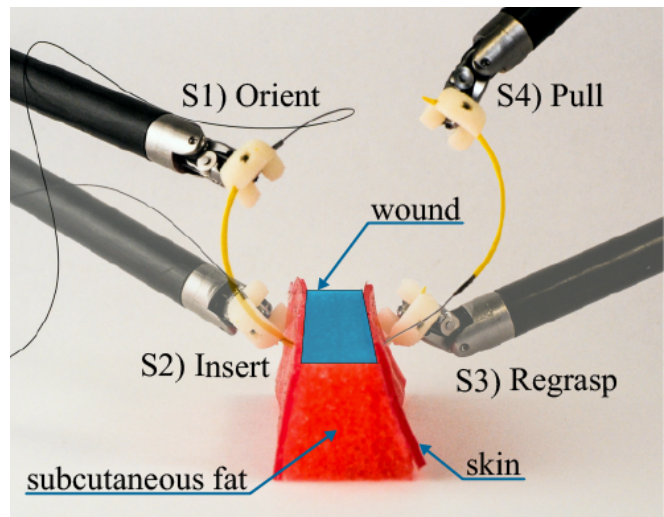

Fig. 1: Each throw in Multi-throw Suturing (MTS) includes five steps: (S1) Needle placement in desired position and orientation by first actuator, (S2) Needle insertion through tissue by first actuator, (S3) Needle grasp by second actuator, (S4) Needle and thread pull until thread is taut, and (S5) Needle transfer back to first actuator. (note: S5 is not illustrated in this time-lapse image).

complete 86% of attempted throws at 30% the speed of human operators [5].

II. Background and Related Work

RSAs are being used for many tumorectomy interventions within the abdominal and thoracic cavities such as prostectomy and hysterectomy [2, 25] as described in reviews of recent developments in semi-autonomous and autonomous execution of surgical procedures by Moustris et al. [20] and Kranzfelder et al. [14].

Automated Suturing: Automation of suturing has been studied in the context of hierarchical models for multi-step task planning [11], multilateral manipulation of needle and suture [34], and interaction with deformable tissue [8, 9].

While each of these studies made significant contributions as outlined below, challenges in combining the steps to achieve autonomy in longer tasks has not been sufficiently addressed. Kang et al. devised a specialized stitching device for RMIS which is capable of tying a knot [11]. Mayer et al. used a recurrent neural net as part of a controller to learn knot tying with three industrial arms using motion primitives from human demonstrations [18]. Van den Berg et al. used iterative learning for performing knot tying at superhuman speeds [36]. More recently, Schulman et al. used a learning by demonstration approach to warp recorded expert demonstrations and perform suturing in simulation [31].

---
* These authors contributed equally to the paper
The authors are with University of California, Berkeley, CA USA 94720
[1]EECS, {siddarthsen, yjen}@berkeley.edu
[2]IEOR & EECS, {animesh.garg, goldberg}@berkeley.edu
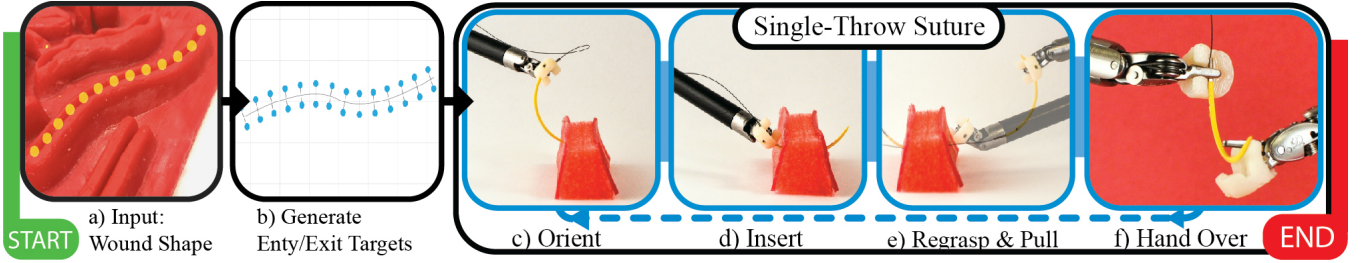[3]Mechanical Engineering, {dgealy, mckinley}@berkeley.edu

Fig. 2: The figure outlines the Multi-Throw Suturing Finite State Machine. First the surgeon specifies a suture path with wound width & depth and suture pitch. The system then computes the number of suture throws required; and generates entry & exit points, and optimized trajectories along with required needle size for each throw of the MTS. Each of the steps S1-S5 (see Figure 1) are repeated with visual feedback for each suture throw until all suture throws are completed.

Padoy et al. showed execution of collaborative human-robot suturing, but the key sections requiring interactions such as needle insertion and hand-off were performed manually [26]. Similarly, Staub et al. automated needle insertion into tissue for single-throw suturing [34].

Prior work in surgical automation has modeled the basis set of surgical motions as the "Language of Surgery" composed of surgemes (Hager et al.) [29]. Recent works have also explored the use of learning techniques to infer surgeme transitions from demonstration data [16, 24]. Many of the FSRS procedures, including MTS, are decomposable into long sequences of simpler sub-tasks. This decomposition allows the parametrization and building of Finite State Machines (FSM) for complex procedures using a learning by observation approach, for tasks such as tissue debridement [13], pattern cutting [21], and tumor localization & resection [19]. Our work on segmentation of multi-step task demonstrations [15] suggests that unsupervised learning of semantic transitions is feasible and can be analyzed to construct FSMs for these multi-step tasks.

Suture Needle Path Planning: Some preceding studies use a needle path of fixed curvature. Jackson et al. used a reference trajectory to create an analytical solution allowing for needle insertion without considering uncertainty or robot pose constraints [9]. However, needles do not always follow their natural curvature. Interaction with tissue may deflect the needle, and end point pose constraints necessitate non-orthogonal exit. The use of optimization-based planning has potential to address these limitations. Recent results in motion planning have shown that Sequential Convex Programming (SCP) based planning, such as [30] can be both faster and more successful in finding solutions than sampling based planners. This paper formulates suture needle path planning as a curvature constrained SCP based optimization problem.

This paper builds on prior work in optimization-based planning [4, 27], sub-task level segmentation of demonstrations [15, 16], gripper mounted interchangeable tools [19], and building robust finite state machines [21]. We are not aware of any system that can perform autonomous multi-throw suturing.

III. PROBLEM: FORMULATION AND DEFINITIONS

The success of suturing is highly sensitive to needle pose uncertainty at entry point. Uncertainty in needle pose during insertion can result in tissue injury due to skin penetration at undesirable angles or the lack of sufficiently deep needle insertion to hold the suture securely. As illustrated by the several error cases in Figure 3, it is essential to maintain proper needle pose during insertion and handover to avoid dropping the needle or damaging tissue. Since the needle is thin and highly reflective, it is difficult to accurately detect its position and orientation with computer vision as noted in [9, 10, 23, 33]. Several medical device manufacturers offer needle-alignment devices for manual laparoscopic applications [17, 28] but, to the best of our knowledge, these are not available for RSAs.

Surgeons follow suturing task guidelines such as entering the tissue orthogonally, minimizing tissue-needle wrench, choosing the correct needle size for adequate suture depth, and inserting the needle to a sufficient depth to ensure needle protrusion for needle re-grasp. While a needle would follow a constant curvature path through rigid objects, tissue is deformable. Thus we model the needle path to allow bounded rotations about the needle tip while the needle is inserted. However, needle paths that do not follow the natural curvature of the needle can result in tissue damage, hence we define a bounded deviation (γ) from needle curvature (κ) that can be visualized as a cone at each point as illustrated in Figure 4. We monotonically reduce γ as the needle progresses to minimize tissue damage.

Assumptions: We assume that tissue is homogeneous and deformable. Teal-time tracking and planning is used to account for departures from needle pose estimates during needle insertion. We assume that the needle is rigidly held in the gripper and can only move forward in the tangential direction of the tip. However, bounded reorientation of the needle tip is permitted as it is inserted through tissue. We assume that our system has access to a continuous range of needle sizes. In practice, needles vary in length in increments of 1 mm and vary in three different fractions of a circle.

Input: The wound shape is provided as input, with the points $\mathcal{M} = [M_1, M_2, \dots, M_D] \in \mathbb{R}^3$ representing the wound surface as a spline. The system is also provided with suture depth d, suture width l, and a pair of entry/exit poses ($P_i, P_f \in SE(3)$) for the first throw as illustrated in Figure 3. Further, we are
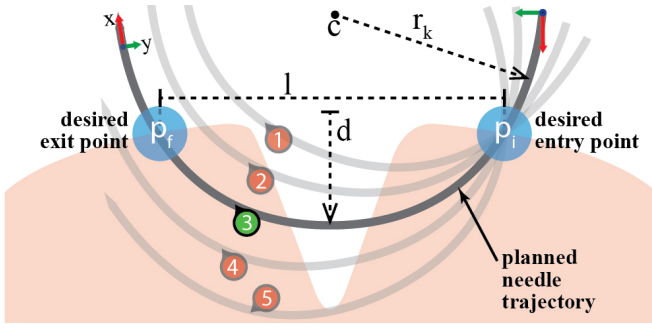
Fig. 3: The needle trajectory labeled (3) shows the desired trajectory along with poses at entry and exit points from the tissue. The success of suturing depends on correct orientation of needle with respect to the tissue. For example, uncertainty in needle pose at entry point may result in the needle not connecting opposite tissue sides (1), not making sufficiently deep insertion to hold the suture securely (2), not having enough length of needle at the other end to enable re-grasping (4), or passing completely under the wound and not exiting the tissue at all (5).

also given suture pitch w – distance between consecutive suture throws.

Output: The system needs to find a set of suture throws $\mathcal{S}$, where $\forall S_j \in \mathcal{S}$, we need to calculate an optimized sequence of needle tip poses $\mathcal{X}_j \in SE(3)$ satisfying the the suture depth and suture width constraints or report that no such path plan exists. The system also needs to choose a needle curvature and length. The entry and exit positions at each suture throw S_j are obtained by linearly interpolating P_i, P_f along the spline while keeping the orientation constant.

Curvature Constrained Kinematic Model:
The needle trajectory is discretized into time intervals $\mathcal{T} = \{0, 1, \ldots, T\}$, where the needle moves a fixed length (Δ) at each time step. At each time step the needle's pose is parametrized as $X_t \in SE(3)$.

We model the needle trajectory as a sequence of $T-1$ circular arcs with curvature κ_t between every consecutive pair of needle poses (X_t, X_{t+1}). We model our control of the needle at each time step as a rotation and insertion where at each time step the pose X_t is propagated a distance Δ to X_{t+1}. Although a needle naturally follows a path of constant curvature, the needle tip can be reoriented at each time step to change the local curvature by $\bar{\gamma}_t$. Thus at each time step the path curvature κ_t can be expressed as $\kappa_t = \kappa + \bar{\gamma}_t$ where κ is the curvature of the needle and $\bar{\gamma}_t$ is the change in curvature applied at each time step. The transformation between consecutive needle poses can be represented a twist in $\mathfrak{se}(3)$, $u_t = \begin{bmatrix} \Delta & 0 & 0 & 0 & \Delta\kappa_t & 0 \end{bmatrix}^T$

The Lie group $SE(3)$ and the corresponding algebra $\mathfrak{se}(3)$ are related by the exponential and log maps $\exp : \mathfrak{se}(3) \to SE(3)$ and $\log : SE(3) \to \mathfrak{se}(3)$. Closed form expressions exist to compute these maps efficiently. Given an incremental twist $x = [p_x \ p_y \ p_z \ r_x \ r_y \ r_z]^T \in \mathbb{R}^6$, the corresponding Lie algebra element is given by the mapping $\wedge : \mathbb{R}^6 \to \mathfrak{se}(3)$ as

$$x^\wedge = \begin{bmatrix} 0 & -r_x & r_y & p_x \\ r_z & 0 & -r_x & p_y \\ -r_y & r_x & 0 & p_z \\ 0 & 0 & 0 & 1 \end{bmatrix}$$
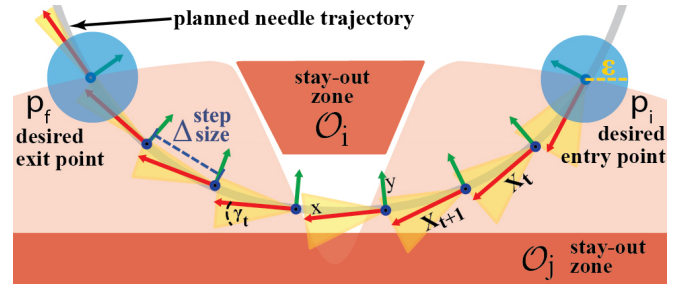

Fig. 4: The optimization steps and non-holonomic motion at each time-step. The figure shows stay-out zones $\mathcal{O}_i$, trajectory poses X_t, step-size Δ, needle radius r, and γ-cone of allowed rotation at each X_t.

The reverse mapping $^\vee : \mathfrak{se}(3) \to \mathbb{R}^6$ can be used to recover the twist, x from an element of $\mathfrak{se}(3)$ Poses between consecutive time steps can then be related as:

$$X_{t+1} = \exp(u_t^\wedge) \cdot X_t \tag{1}$$

.

IV. SUTURE NEEDLE PATH PLANNING

The Suture needle Path Planning (SPP) problem can be formulated as a non-convex, curvature constrained motion planning problem solved with a series of locally convex approximations using sequential convex programming (SCP). We begin by presenting the problem formulation.

Optimization Model:
For notational convenience we concatenate the states from all time steps as $\mathcal{X} = \{X_t : t \in \mathcal{T}\}$ and control variables as $\mathcal{U} = \{\kappa, \Delta, \gamma_t : t \in \mathcal{T}\}$

$$SPP : \underset{\mathcal{X}, \mathcal{U}}{\text{minimize}} \quad \alpha_\Delta \mathcal{C}_\Delta + \alpha_I C_I \tag{2}$$

$$\text{s.t.} \quad \log(X_{t+1} \cdot (\exp(u_t) \cdot X_t)^{-1})^\vee = 0_6 \tag{3}$$

$$|\bar{\gamma}| \leq \gamma_t \quad \forall t \tag{4}$$

$$T\Delta + 2l_g - \frac{2\pi l_n}{\kappa} \leq 0 \tag{5}$$

$$\text{sd}(X_t, \mathcal{O}_i) \geq d_s, \quad \forall i \tag{6}$$

$$X_0 \in \mathcal{B}(p_i, \varepsilon), \ X_T \in \mathcal{B}(p_f, \varepsilon) \tag{7}$$

Each term in the above formulation is described below:

Costs (Eqn. 2): We assume the volume of needle in tissue is proportional to tissue trauma and hence we penalize longer trajectories such that $C_\Delta = T\Delta$, the length of the trajectory. Furthermore, surgical guidelines suggest that the needle entry pose should be orthogonal to the tissue surface. C_I penalizes deviations from an orthogonal start pose. The weights α_Δ and α_I are parameters that are tuned in the optimization.

Kinematic Constraints (Eqns. 3, 4): The kinematic constraint in Eqn. 1 can be transformed using the exponential log map into the standard equality constraint in Eqn. 3. Eqn. 4 bounds the magnitude of $\bar{\gamma}_t$ to minimize tissue damage. We select γ_t to be monotonically decreasing with t because needle rotations away from its natural curvature cause greater damage the further the needle is inserted into tissue.

Needle Length Constraints (Eqn. 5): The length of the insertion trajectory ($T\Delta$) is constrained to be less than the
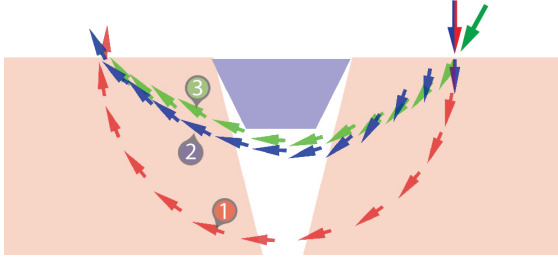
Fig. 5: The side view of three needle trajectories generated by SPP. Trajectory 1 and 3 are constant curvature trajectories whereas trajectory 2 is a variable curvature trajectory.

length of the needle $(2\pi l_n/\kappa)$ and should allow for grippers to hold the needle on both ends $(2l_g)$.

Collision Constraints (Eqn. 6): We impose constraints to ensure that our trajectory avoids collisions with pre-defined stay out zones. We ensure that the signed distance between each X_{t+1} and each convex mesh in $\mathcal{O}$ is greater than a safety margin parameter d_s. The stay out zones can be non-convex meshes that can be decomposed into convex sub meshes [3], $\mathcal{O} = \{\mathcal{O}_1, \ldots, \mathcal{O}_i\}$.

Entry and Exit Point Constraints (Eqn. (7)): We constrain the start and end poses of the trajectory to be within an ε-Ball of the calculated entry (p_i) and exit (p_f) poses. This can be expressed as $\log(p_i \cdot X_0^{-1})^\vee \leq \varepsilon \cdot \mathbf{1}_6$ for the start pose of the trajectory. The end pose constraint follows a symmetric formulation.

We note that a constant of Δ is chosen for all time steps instead of having a different Δ_t for each time. as the latter is experimentally found to disagree numerically with the findings of Duan et al. [4].

Trajectory Optimization
Sequential convex programming is a general approach for solving constrained, non-convex optimization problems. We refer the reader to [32] for the details of SCP-based motion planning are described.

Figure 5 shows the SPP output for three different sets of pose constraints. For #1, we restrict rotation about needle tip ($\gamma_t = 0, \forall t$). Coupled with the orthogonality constraint at entry/exit, this results in a constant curvature path along the needle radius. For #2, orthogonality is enforced only at entry pose, and γ_t is set to a monotonically decreasing sequence in t. This results in rotations about the needle tip that achieve an asymmetric trajectory satisfying pose constraints at entry. We also demonstrate a case with no pose constraints in #3, resulting in the shortest path trajectory, but with oblique entry angles.

V. Reducing Needle Pose Uncertainty

As stated in Section III and Figure 3, tissue damage is minimized with orthogonal needle entry and motions that are tangential to the needle tip. These guidelines require accurate needle pose estimates at the needle entry point and robust needle grasps.

A. Suture Needle Angular Positioner (SNAP)

Commercially available RMIS needle drivers allow handling of a variety of needle sizes, however an analysis of

suturing trials in JIGSAWS dataset [5] reveals that multiple pairs of hand-offs are required for correct needle orientation. This is because the motion of a needle held within the needle driver jaws is not fully constrained. The flat gripper surface allows rotation and translation along the length of the needle, which can be hard to control without haptic or visual feedback.

There have been some commercial efforts to mitigate back-and-forth hand-offs and uncertainty in laparoscopic surgery through passively orienting the needle on gripper closure using a "self-righting" gripper jaw design [17, 28]. However, these are not designed for automation, and require a complete tool redesign.

We develop a design for a low-cost Suture Needle Angular Positioner (SNAP) for dVRK Classic 8 mm Needle Driver with 6 mm jaws, which works to guide and passively orient a curved needle into a stable pose upon closure of gripper jaws as illustrated in Figure 6(d). SNAP reduces needle pose uncertainty along two rotational axes as shown in Section VII. This allows for a higher tolerances in relative positioning during needle hand-off, and which relaxes the accuracy requirements of needle tracking.

Mode of Operation: SNAP is mounted axially on one of the needle driver jaws. It is designed to guide the needle towards a groove running perpendicular to the length of the gripper jaws Figure 6(b), (c). Upon closing the jaws, the needle rolls to a stable pose, passing through contact points C_1 and C_2 as shown in the section view in Figure 6(b).

The size of the needle gripper is parametrized by the distance between contact points C_1 and C_2 which is dependent on the curvature of the needle, that is a needle with a larger radius needs a wider contact grasp to enable the needle rolling upon jaw closure. As illustrated in Figure 6 (a), SNAP has a rear-wall that allows the gripper to overshoot during the pre-grasp approach. It also has a needle *catching area* in the front (Figure 6 (c)) that guides the needle into the groove, compensating for undershoot during pre-grasp. Both of the above features increase the robustness of needle manipulation.

The SNAP is fabricated from ABS plastic using a *Stratasys uPrint* 3D printer. For an 8 mm classic needle driver, using a $\frac{3}{8}$ circumference, 39 mm length needle, we designed the SNAP with $C_1 - C_2$ span of 10 mm. Through experimental evaluation, we improved upon the SNAP design to include a larger rear wall. This enabled a wider jaw opening during approach allowing for larger tolerance in needle pose uncertainty.

B. Real Time Needle Tracking

We have developed a real-time needle tracking system to provide closed loop feedback during the suturing process as summarized in Figure 7. Due to tissue and tool specularity, perception using RGB-D sensing is not feasible. Our system provides 3D needle pose estimates using a custom built stereo camera pair, composed of two Prosilica GigE GC1290C cameras with 6 mm focal length lenses. The needle tracking algorithm is implemented as a ROS node
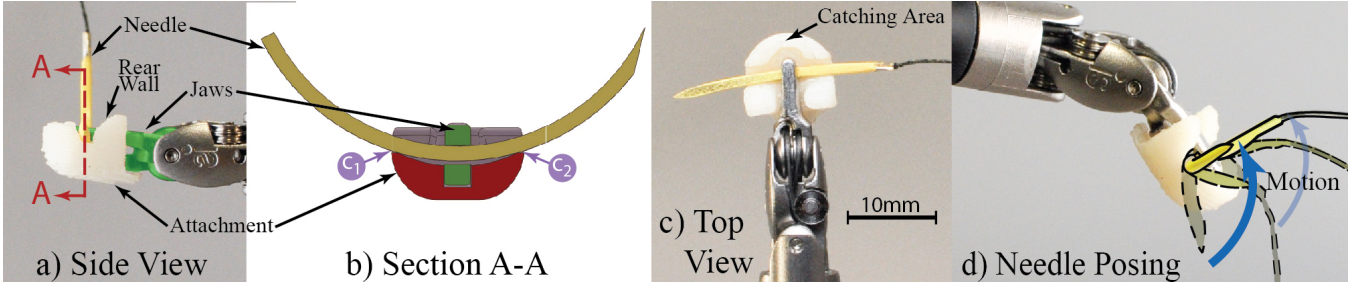
Fig. 6: This figure illustrates the design and function of the 3D-printed Suture Needle Angular Positioner (SNAP). Figures (a) and (b) show a convex depression in which needle rests upon gripper closure. Figure (d) shows a time-lapse figure of the gripper closing action on needle orientation.
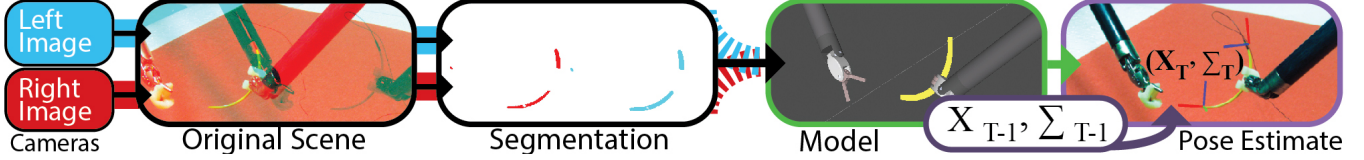

Fig. 7: This figure shows an overview of the needle tracking pipeline, from stereo images to the final needle pose estimate overlaid onto the original scene. We fuse a Kalman Filter estimate with current camera estimate to compute the final estimate. The tracking system is robust to outliers and missing data in the segmentation masks.

that publishes real time estimates of the needle's pose. The tracking system works with partial occlusion for instance when the needle is inside the tissue or behind the robot arms.

We use a model-based tracking system leveraging the needle shape and color. The first step in the process is *Needle Segmentation*. We use a yellow painted needle to assist in foreground/background separation. We use HSV (Hue, Saturation, Value) separation to identify the needle in a cluttered environment with the open-source OpenCV library and create a set of image plane points $\mathcal{P}_I$.

We leverage the circular shape of the surgical needles and their elliptical projection. We create a small set of parametrically sampled points along the length of needle model $\mathcal{P}_M$, $|\mathcal{P}_M| = 12$, and then use affine point set registration to fit the $\mathcal{P}_I$ to $\mathcal{P}_M$. We model the non-linear registration problem as point set matching. This creates robustness to outliers, missing data due to occlusions, and noisy data from incorrect segmentation masks. We use the Matlab library CPD2 for solving the registration problem [22].

Using the ellipse fits on the image pair, we generate a dense set of corresponding points along the needle. This creates a robust disparity map of 3D points on the needle. A plane is then fit to the 3D points, providing a normal vector, while an average tangential direction is calculated using the three points on the end of the needle. Using the end point of the needle and these two vectors, a pose $p_n \in \mathbb{R}^6$ is generated. We use a Kalman filter to smooth needle tip pose estimates.

The use of industrial Prosilica cameras with a wide baseline necessitated the use of a large workspace and consequently larger than average needles in order to enable robust needle tracking. Laparoscopic cameras have a smaller baseline and smaller field of view compared to our setup. The proposed tracking system should be transferable to a laparoscopic setup allowing the use of much smaller needles.

VI. Multi-Throw Suturing: System Design

We present a closed loop Finite State Machine (FSM) for multi-throw suturing with needle orientation tracking and multilateral needle hand-off as illustrated in Figure 2. Given the registration of the tissue phantom in the camera frame, a multi-throw suture plan is generated. The SPP algorithm is used to generate needle trajectories and a suggested needle curvature. Each throw in the task consists of the following sequence of sub-tasks which were segmented on the basis of manual surgeme labels for suturing in the JIGSAWS dataset:

S1. Needle Orientation: The system generates pose estimates for both the front tip of the needle, N_T, and the tail connected to the suture thread, N_S. Starting with the needle held in the right gripper at N_S, the system creates an initial pose estimate. Using this estimate, the robot aligns the needle with the camera's image plane, allowing for an occlusion-free view of the needle and an improved pose estimate.

S2. Needle Insertion: The system executes a trajectory for N_T using the planner described in the previous section. We note that at this point, suture path can be re-planned after every user-specified rolling time horizon.

S3. Needle Grasp: After the right arm guides the needle through tissue, the left arm grasps the needle at N_T and pulls the needle tangentially to the needle tip, rotating around the center of curvature of the needle in order to minimize tissue trauma.

S4. Needle Pull: Once the needle is completely outside the tissue, it is pulled away sufficiently to tighten the suture. The system estimates how much slack is available in the suture thread by modeling the length of thread between consecutive entry points as a helical loop with radius equal to the radius of the needle and pitch equal to the suture pitch. This provides a conservative estimate of how much slack is lost in each throw and the system uses it to decrease the distance the needle is pulled away after each throw.

S5. Needle Hand-Off: Our needle tracking algorithm estimates the pose of the needle end N_S while it is grasped at N_T. Similar to step (S1), the left arm aligns the needle with the image plane to improve the needle pose estimate. This estimate is used to align the needle with the right arm in order to grasp the needle at N_S and perform the next suture throw.

Due to inherent pose errors in camera-robot registration and robot kinematics, the hand-off process is performed by simultaneously engaging the right arm at N_S while disengaging the left arm at N_T. A slight error in coordination will result in failed transfer due to stresses generated on the needle. The use of SNAP on both gripper ends facilitates this process because the grooves provide a space resulting in a partial cage instead of force closure during the hand-off as described in Section V.

VII. Initial Experiments

A. dVRK: Hardware and Software

We use the Intuitive Surgical da Vinci Research Kit (dVRK) surgical robot assistant as in [21], along with open-source electronics and software developed by WPI and Johns Hopkins University [12]. We use a pair of 8mm Needle Drivers with each gripper having one Suture Needle Angular Positioner (SNAP). The software system is integrated with ROS and allows direct robot pose space control, working in Cartesian space instead of commanding motor torques.

B. Experimental Evaluation of Needle Tracking

The size and shape of needles makes it difficult to obtain ground truth pose estimates using techniques like fiducial-based motion capture. Instead we designed an experiment to indirectly verify the efficacy of our needle tracking system. The robot holds the needle rigidly in its gripper and moves the needle to random positions in the workspace. Note that the relative pose of the needle with respect to the gripper position never changes. At each random position the robot pauses and uses the needle tracking system to compute the needle's relative pose with respect to the gripper pose (estimated from kinematics). Poses at 20 different random locations were recorded. Table I shows the standard deviation in x,y,z (in mm) and in roll, pitch, and yaw (in degrees) respectively in the needle's relative pose. The low error in every dimension suggests that our estimates of the needle's relative pose are nearly identical at each random location. This matches with the ground truth that the needle's relative pose never changes. The errors reported are not due to the needle tracker alone, but the composite error produced from needle tracking, camera-robot registration, and robot kinematics. However, the errors provide an upper bound on the needle tracking error and is representative of error that our system must be robust to.

TABLE I: Error in Relative Needle Pose (Over 20 Trials)

	Position (mm)			Orientation (degrees)		
	x	y	z	Yaw	Pitch	Roll
Std. Dev.	2.182	1.23	1.54	2.495	4.699	4.329

TABLE II: SNAP Evaluation

Stationary Grasp Orientation	Error (Standard Deviation)						
	Succ. Grasps	x (mm)	y (mm)	z (mm)	yaw (deg)	pitch (deg)	roll (deg)
Without SNAP	100%	2.511	1.434	4.838	20.547	7.584	6.472
With SNAP	100%	0.199	0.158	0.177	0.926	1.094	0.664
Perturbed Grasp Orientation	Error (Standard Deviation)						
	Successful Grasps	x (mm)	y (mm)	z (mm)	yaw (deg)	pitch (deg)	roll (deg)
Without SNAP	100%	2.01	2.59	5.95	15.54	12.74	7.62
With SNAP	91.66%	1.58	1.15	1.19	5.55	3.97	6.34

C. Evaluation of Suture Needle Angular Positioner (SNAP)

1. Stationary Needle Pick up: In this experiment we evaluate the SNAP's ability to reduce variation in needle grasp pose. This variation is the result of small natural perturbations in the needle starting pose and noise in the robot's kinematic chain. In each trial, a needle is placed in the same location and the robot is provided a constant known grasp pose to initiate pick up. Once the needle is grasped, the robot brings the needle to a known location and the needle's pose is recorded using our needle tracker. We repeat this process over ten trials both with and without SNAP. The standard deviations in each degree of freedom of the needle's pose is presented in Table II. The SNAP reduced needle pose variation in both position and orientation, in some cases by over one order of magnitude.

2. Perturbed Needle Pick up: In the second experiment we intentionally perturb the orientation of the robot's grasp pose to evaluate robustness to uncertainty and variation in grasp orientation. Experiment 2 is a variation of experiment 1 where the commanded grasp pose is perturbed from -30 degrees to 30 degrees in yaw, pitch, and roll. The perturbations are applied in increments of 10 degrees independently in each axis resulting in 19 trials total. Our results show that the use of SNAP results in a 3x reduction in needle pose uncertainty over the standard Needle Driver.

D. Robot Experiments: Four-Throw Suturing Task

We used a suturing phantom made with foam to mimic subcutaneous fat tissue with a layer of 1mm thick skin using (shore hardness 2A) *DragonSkin 10 Medium* Silicone Rubber (*Smooth-On*). The soft tissue phantom deforms during needle insertion to introduce uncertainty. The mechanical design of the dVRK robotic arms ensure that the arms do not move at the point where they would enter a human body ensuring that the kinematic motions of our system remain feasible in-vivo in a minimally invasive surgical (MIS) setting. Due to the wide baseline of our stereo cameras, the size of our phantom, needles, and workspace were constrained to be larger than those found in a nominal MIS setting.

In this experiment, the system tries to complete a closed loop four throw suturing task similar to the suturing task found in the JIGSAWS data-set [5]. We initialized the system with entry and exit poses on opposite surfaces of the tissue phantom and with a desired suture depth. Our system generates insertion trajectories and based on the output optimal needle curvature we selected a 39 mm long, 3/8 reverse cutting needle to perform the suturing throws. For each trial

TABLE III: Results for Four-Throw Suturing. 14 trials were performed, with a 50% success rate. For failed states, "N.I" represents incorrect needle orientation or insertion, "G.P." represents incorrect needle re-grasp and pull after insertion, and "H.O" represents failure in needle hand-off respectively. The test setup was varied with translation of simulated wound along the wound axis.

Trial	4-Throw Success	# of Throws Completed (Attempted)	Failure Mode	Trans. in X	Suture Pitch	Total Time(s)
1	Failure	1 (2)	G.P.	-3mm	3mm	-
2	Failure	2 (3)	G.P.	-3mm	3mm	-
3	Failure	3 (4)	G.P.	-2mm	3mm	-
4	Success	4 (4)		-1mm	3mm	387
5	Success	4 (4)		0mm	3mm	380
6	Success	4 (4)		0mm	3mm	380
7	Success	4 (4)		0mm	3mm	383
8	Failure	2 (3)	H.O.	1mm	3mm	-
9	Failure	2 (3)	N.I.	1mm	3mm	-
10	Failure	3 (4)	G.P.	2mm	3mm	-
11	Success	4 (4)		3mm	3mm	393
12	Success	4 (4)		4mm	3mm	383
13	Success	4 (4)		5mm	3mm	382
14	Failure	3 (4)	G.P.	6mm	3mm	-
Mean	50%	3.14				384
Std Dev		1.027		Single Throw Success Rate: 86.3%		

TABLE IV: This table compares the performance of our autonomous suturing system with different skill levels of surgeons in the JIGSAWS dataset[5]

Operator Mode	Average Time for 1-Throw (s)	Average time for 4-throw Task (s)
Expert	19.03	87.02
Intermediate	18.57	87.89
Novice	32.14	136.85
Autonomous (Our Approach)	112.33	383.00

we record time to completion as well as the failure mode if necessary. The robot moves at a top speed of 3cm/s. The results of each trial are found in Tables III and IV.

VIII. DISCUSSION AND FUTURE WORK

Initial experiments in this paper confirm that the system presented can computationally plan and execute multi-throw suturing task with four-throws in closed-loop operation. The combination of our needle tracking system and the SNAP enables our system to minimize and be robust to needle pose uncertainty. This allows our system to perform multilateral needle hand-off, enabling the execution of multi-throw suturing.

The system completes 86.3% of individual suture throws attempted at approx. 30% of the average speed of manually tele-operated demonstrations as listed in Tables III and IV. Our results also show that the proposed needle tracking system can provide robust estimates of needle pose in near real-time with an empirical error of up to 5 degrees. Furthermore the use of SNAP improves repeatability in needle grasping by $10\times$ and grasping is robust to up to 30 degrees error in needle estimate.

However, we note that the system completes on average 3.14 of the intended 4 throws, with a 50% completion rate for the four-throw task. It is worth noting that 5 out of the 7 failures were due to incorrect needle re-grasp and pulling after the insertion step. Some of these failures were due to incorrect needle estimate after the needle exits the tissue in unexpected locations. The visual needle tracker could not recognize the needle due to large occlusions. Additional failures were due to entanglement of the suture thread during the needle pulling.

The slow speed of the task execution is partly because of the larger workspace as compared to the setup in JIGSAWS data [5]. Furthermore, moving to align the needle in camera for improving needle pose also contributes to the delay. We will work to improve the real-time visual estimate of the needle pose without the need for explicit alignment in front of the camera. Future work will focus on improving needle pose estimation with very large occlusions along with receding horizon re-planning during the needle insertion to reduce error in needle re-grasp. We will also evaluate the use of swept needle volume as objective cost and explore augmenting the needle state with needle pose belief for uncertainty compensation through optimization re-planning.

This paper presents initial results toward automating MTS with a combination of new hardware and a novel optimization algorithm. The paper describes the mechanical device, the Suture Needle Angular Positioner (SNAP), designed to align and hold the needle in a known orientation, and an SCP formulation of needle motion planning. Initial results suggest that SNAP can reduce error in needle orientation by $3\times$ and that the combined system can successfully complete 86% of attempted throws at 30% the speed of human operators [5].

One challenge is the unpredictability of suture thread. The thread we used is very difficult to track with computer vision and has high friction with tissue phantoms. We are currently exploring ex-vivo experiments with chicken tissue which has natural lubrication that lowers friction.

REFERENCES

[1] J. M. Burch, R. J. Franciose, E. E. Moore, W. L. Biffl, and P. J. Offner, "Single-layer continuous versus two-layer interrupted intestinal anastomosis: a prospective randomized trial," *Annals of surgery*, 2000.

[2] A. Darzi and Y. Munz, "The impact of minimally invasive surgical techniques," *Annu. Rev. Med.*, 2004.

[3] F. De Goes, S. Goldenstein, and L. Velho, "A hierarchical segmentation of articulated bodies," in *Computer Graphics Forum*, 2008.

[4] Y. Duan, S. Patil, J. Schulman, K. Goldberg, and P. Abbeel, "Planning locally optimal, curvature-constrained trajectories in 3D using sequential convex optimization," in *2014 IEEE International Conference on Robotics and Automation (ICRA)*, 2014.

[5] Y. Gao, S. Vedula, C. Reiley, N. Ahmidi, B. Varadarajan, H. Lin, L. Tao, L. Zappella, B. Bejar, D. Yuh, C. Chen, R. Vidal, S. Khudanpur, and G. Hager, "The JHU-ISI Gesture and Skill Assessment Dataset (JIGSAWS): A Surgical Activity Working Set for Human Motion Modeling," in *Medical Image Computing and Computer-Assisted Intervention (MICCAI)*, 2014.

[6] J. Hochberg, K. M. Meyer, and M. D. Marion, "Suture choice and other methods of skin closure," *Surgical Clinics of North America*, vol. 89, no. 3, pp. 627–641, 2009.

[7] Intuitive Surgical, "Annual report 2014." [Online]. Available: http://investor.intuitivesurgical.com/phoenix.zhtml?c=122359&p=irol-IRHome

[8] M. C. Jackson, Russell C.and Cavusoglu, "Modeling of needle-tissue interaction forces during surgical suturing," in *2012 IEEE International Conference on Robotics and Automation (ICRA)*, 2012.

[9] R. C. Jackson and M. C. Cavusoglu, "Needle path planning for autonomous robotic surgical suturing," in *Proc. IEEE Int. Conf. Robotics and Automation (ICRA)*, 2013.

[10] R. C. Jackson, R. Yuan, D.-L. Chow, W. Newman, and M. C. Cavusoglu, "Automatic initialization and dynamic tracking of surgical suture threads," in *IEEE Int. Conf. Robotics and Automation*, 2015.

[11] H. Kang and J. T. Wen, "Autonomous suturing using minimally invasive surgical robots," in *Control Applications, 2000. Proceedings of the 2000 IEEE International Conference on*. IEEE, 2000, pp. 742–747.

[12] P. Kazanzides, Z. Chen, A. Deguet, G. Fischer, R. Taylor, and S. DiMaio, "An Open-Source Research Kit for the da Vinci Surgical System," in *IEEE Int. Conf. Robotics and Automation (ICRA)*, 2014.

[13] B. Kehoe, G. Kahn, J. Mahler, J.-H. Kim, A. Lee, A. Lee, K. Nakagawa, S. Patil, W. D. Boyd, P. Abbeel, and K. Goldberg, "Autonomous multilateral debridement with the Raven surgical robot," *Robotics and Automation (ICRA), 2014 IEEE International Conference on*, 2014.

[14] M. Kranzfelder, C. Staub, A. Fiolka, A. Schneider, S. Gillen, D. Wilhelm, H. Friess, A. Knoll, and H. Feussner, "Toward increased autonomy in the surgical or: needs, requests, and expectations," *Surgical endoscopy*, vol. 27, no. 5, pp. 1681–1688, 2013.

[15] S. Krishnan*, A. Garg*, S. Patil, C. Lea, G. Hager, P. Abbeel, and K. Goldberg (*denotes equal contribution), "Transition state clustering: Unsupervised surgical trajectory segmentation for robot learning," in *Int. Sym. of Robotics Research*. Springer STAR, 2015.

[16] C. Lea, G. D. Hager, and R. Vidal, "An improved model for segmentation and recognition of fine-grained activities with application to surgical training tasks," in *Applications of Computer Vision (WACV), 2015 IEEE Winter Conference on*. IEEE, 2015, pp. 1123–1129.

[17] D. Martin, J. Woodard, C. Shurtleff, and A. Yoo, "Articulating needle driver," Nov. 15 2012, US Patent App. 13/466,188.

[18] H. G. Mayer, F. J. Gomez, D. Wierstra, I. Nagy, A. Knoll, and J. Schmidhuber, "A System for Robotic Heart Surgery that Learns to Tie Knots Using Recurrent Neural Networks." *IROS*, 2006.

[19] S. McKinley, S. Sen, A. Garg, Y. Jen, D. Gealy, P. Abbeel, and K. Goldberg, "Autonomous Tumor Localization and Extraction: Palpation, Incision, Debridement and Adhesive Closure with the da Vinci Research Kit," Hamlyn Surgical Robotics Conference, London.

[20] G. Moustris, S. Hiridis, K. Deliparaschos, and K. Konstantinidis, "Evolution of Autonomous and Semi-Autonomous Robotic Surgical Systems: A Review of the Literature," *Int. Journal of Medical Robotics and Computer Assisted Surgery*, vol. 7, no. 4, pp. 375–392, 2011.

[21] A. Murali*, S. Sen*, B. Kehoe, A. Garg, S. Patil, W. D. Boyd, S. Lim, P. Abbeel, and K. Goldberg, "Learning by Observation for Surgical Subtasks: Multilateral Cutting of 3D Viscoelastic and 2D Orthotropic Tissue Phantoms," in *IEEE Int. Conf. Robotics and Automation*, 2015.

[22] A. Myronenko and X. Song, "Point set registration: Coherent point drift," *IEEE Tran. on Pattern Analysis and Machine Intelligence*, 2010.

[23] F. Nageotte, C. Doignon, M. de Mathelin, P. Zanne, and L. Soler, "Circular needle and needle-holder localization for computer-aided suturing in laparoscopic surgery," pp. 87–98.

[24] S. Niekum, S. Osentoski, G. Konidaris, S. Chitta, B. Marthi, and A. G. Barto, "Learning Grounded Finite-State Representations from Unstructured Demonstrations," *Int. J. of Robotics Research*, 2015.

[25] C. C. L. or Open Resection Study Group *et al.*, "Laparoscopic surgery versus open surgery for colon cancer: short-term outcomes of a randomised trial," *The lancet oncology*, 2005.

[26] N. Padoy and G. Hager, "Human-Machine Collaborative Surgery using Learned Models," in *Proc. IEEE Int. Conf. Robotics and Automation (ICRA)*, 2011, pp. 5285–5292.

[27] S. Patil, Y. Duan, J. Schulman, K. Goldberg, and P. Abbeel, "Gaussian belief space planning with discontinuities in sensing domains," in *Proc. IEEE Int. Conf. Robotics and Automation (ICRA)*, 2014.

[28] S. Qureshi, K. Rupp, and B. Thompson, "Needle holder with suture filament grasping abilities," Sept. 14 1999, uS Patent 5,951,587.

[29] C. E. Reiley and G. D. Hager, "Task versus Subtask Surgical Skill Evaluation of Robotic Minimally Invasive Surgery," in *Medical Image Computing and Computer-Assisted Intervention (MICCAI)*, 2009.

[30] J. Schulman, Y. Duan, J. Ho, A. Lee, I. Awwal, H. Bradlow, J. Pan, S. Patil, K. Goldberg, and P. Abbeel, "Motion planning with sequential convex optimization and convex collision checking," *The International Journal of Robotics Research*, 2014.

[31] J. Schulman, A. Gupta, S. Venkatesan, M. Tayson-Frederick, and P. Abbeel, "A case study of trajectory transfer through non-rigid registration for a simplified suturing scenario," 2013.

[32] J. Schulman, J. Ho, A. Lee, H. Bradlow, I. Awwal, and P. Abbeel, "Finding Locally Optimal, Collision-Free Trajectories with Sequential Convex Optimization," in *Robotics: Science and Systems (RSS)*, 2013.

[33] S. Speidel, A. Kroehnert, S. Bodenstedt, H. Kenngott, B. Mueller-Stich, and R. Dillmann, "Image-based tracking of the suturing needle during laparoscopic interventions," in *SPIE Medical Imaging*, 2015.

[34] C. Staub, T. Osa, A. Knoll, and R. Bauernschmitt, "Automation of tissue piercing using circular needles and vision guidance for computer aided laparoscopic surgery," in *Robotics and Automation (ICRA), 2010 IEEE International Conference on*, 2010.

[35] A. P. Stegemann, K. Ahmed, J. R. Syed, S. Rehman, K. Ghani, R. Autorino, M. Sharif, A. Rao, Y. Shi, G. E. Wilding, *et al.*, "Fundamental skills of robotic surgery: a multi-institutional randomized controlled trial for validation of a simulation-based curriculum," *Urology*, 2013.

[36] J. van den Berg, S. Miller, D. Duckworth, H. Hu, A. Wan, X.-Y. Fu, K. Goldberg, and P. Abbeel, "Superhuman performance of surgical tasks by robots using iterative learning from human-guided demonstrations," *Robotics and Automation (ICRA), 2011 IEEE International Conference on*, 2010.